Case Study

Figs. 4a and 4b constitute the nomogram with respect to the optimal set of parameters. Figs. 4c and 4d are helpful in quickly reading the values of individual variables that compose the parameters. From Figs. 4a and 4b it can be seen that for given engagement parameters (i.e., γ and V/R) the minimum dwell time available is controlled by a/r. Three cases are considered here for illustration.

Case 1. Worst Case

Let us assume that the requirement is to ensure a minimum dwell time of 100 ms for a typical encounter geometry and $V/R = 0.2$ rad/s. Thus, starting from $V/R = 0.2$ rad/s in Fig. 4a and $t_{\min} = 100$ ms in Fig. 4b, and following the route shown as case 1, point Z is located in Fig. 4b. The value chosen for γ is 0 because it gives minimum dwell time. At point Z, a/r is 0.71. To find the value of a assume an acquisition range of 10 km. Then, following the case 1 route in Figs. 4c and 4d, for $a/r = 0.71$, $a = 500$ m. A value for V/R less than 0.2, however, would lead to a higher value of a for the same R and $t_{\min}$.

Similarly, any constraint on the lowest value of γ would also result in an increment in a/r and, therefore, in a. It can also be noted here that the chance of $\phi = 0$ deg would also be low, and that for $\phi > 0$, the dwell time would always be more than that read by the nomogram. For $\phi > 0$, Eq. (11) can be used.

Case 2. Typical Case

Let $R = 10$ km, $V = 1000$ m/s, and $\gamma = 50$ deg. In this case the minimum dwell time requirement of 100 ms can be met only for cases with $a/r \leq 0.9$ following the case 2 route from Fig. 4c to 4a to 4b. From Fig. 4d, a is found as 630 m.

Case 3. Zero Closing Speed Case

In this case, V is orthogonal to the R vector (i.e., OX or the seeker line of sight). From Fig. 2b

$$\gamma_{\text{orth}} = \tan^{-1}\left(\frac{b}{ON}\right) = \tan^{-1}\left(\frac{a\cos\phi}{R\sqrt{1-(a/R)^2\cos^2\phi}}\right)$$

For a radially outward moving target, $\phi = 0$ and then

$$\gamma_{\text{orth}} = \tan^{-1}\left(\frac{a}{\sqrt{R^2-a^2}}\right) = \tan^{-1}\left[(a/r)\tan\beta\right]$$

In this case, for a target sighted at the beam center (i.e., $a = 0$) $\gamma_{\text{orth}} = 0$; and from Eq. (12)

$$t_{\text{dwell}} = \frac{r}{V} = \frac{\tan\beta}{V/R} = \frac{\text{½ beam width}}{\text{line-of-sight rate}}$$

This would be found in the nomogram by extending graph b in Fig. 4 for the $a/r = 0$ case. It should be noted that when closing speed is zero, Doppler shift is zero. In fact, in this case R is defined as the miss distance. Also, in general, line-of-sight rate = (component of $\bar{V}$ orthogonal to line-of-sight)/R $= [V\cos(\gamma - \gamma_{\text{orth}})]/R$.

Conclusion

A nomogram has been designed to define the circular area within which to find the target for a wide range of missile engagement parameters, given a dwell time constraint.

References

[1]Kuno, H., Nakajima, H., and Ueno, Y., "Mid-Course Guidance for Fire and Forget Missile—Modification of Present Homing Missile," *MEDE Conference Proceedings,* Interania S.A., Geneva, Switzerland, 1979, pp. 597-608.

[2]Kouba, J. T., and Bose, S. C., "Terminal Seeker Pointing-Angle Error at Target Acquisition," *IEEE Transactions on Aerospace and Electronics System,* Vol. AES-16, No. 3, May 1980, 313-319.

[3]Asthana, C. B., and Prahlada, "Evaluation of Missile Seeker Dwell Time for Three-Dimensional Aerial Engagements," *Proceedings of the AIAA Guidance, Navigation, and Control Conference,* AIAA, Washington, DC, 1989, pp. 506-509 (AIAA Paper 89-3484).

Effect of Actuator Coupling on Active Vibration Control of Flexible Structures

Jeffrey B. Horner*
Lockheed Missiles and Space Company, Sunnyvale, California 94089
Daniel J. Rutterman†
Siecor Corporation, Hickory, North Carolina 28603
and
Peter H. Meckl‡
Purdue University, West Lafayette, Indiana 47907

Introduction

THE control of vibration in large structures is complicated by the presence of many closely-spaced modes within the controller bandwidth. Problems of stability robustness arise since accurate models for the entire structure are difficult to generate. This Note investigates stability issues associated with a decentralized control strategy applied to subsystem models of the structure, focusing on the case when subsystem frequencies are closely spaced. Subsystem interaction is assumed to exist primarily because of the actuators, whose locations are usually constrained by physical limitations.

An excellent overview of decentralized control approaches has been written by Sandell et al.[1] One of the first papers to specify conditions for the existence of a local output feedback law was written by Wang and Davison.[2] Conditions on the coupled system dynamics to guarantee stability for decentralized controllers have been developed by Nwokah and Perez.[3] Iftar and Özgüner[4] have proposed a design method for decentralized controllers based on linear quadratic Gaussian/loop transfer recovery (LQG/LTR) techniques.

The work presented in this Note addresses the issue of decentralized control stability for systems having significant subsystem interaction. A novel coupling parameter is introduced that characterizes the degree of subsystem interaction in a 2×2 system that is coupled by the actuator forces. This parameter is used to determine stability bounds for both decentralized and centralized active vibration control. A simple cantilever beam structure with attached disk is used to confirm the theoretical development experimentally.

Stability Analysis

A specific class of structural systems will be considered whose subsystems interact only through the applied forces. The equations of motion for a general structural system model coupled only through the actuators can be represented as follows:

$$I\ddot{Y} + [\,2\zeta_i\omega_i\,]\dot{Y} + [\,\omega_i^2\,]Y = PF \tag{1}$$

where $[\,2\zeta_i\omega_i\,]$ and $[\,\omega_i^2\,]$ represent diagonal matrices that depend on the damping ratio ζ_i and natural frequency ω_i and P represents a nondiagonal coupling matrix.

Before a suitable stability analysis can be developed, Eq. (1) must be converted into transfer matrix form by taking the

Received April 25, 1992; revision received Feb. 18, 1993; accepted for publication Feb. 19, 1993.

*Engineer, P.O. Box 3504, Mail Stop O-7750, B-579.
†Engineer, 489 Siecor Park.
‡Assistant Professor, 1288 Mechanical Engineering Building.

Laplace transform of both sides. The resulting transfer matrix $G(s)$ relating $Y(s)$ to $F(s)$ can be expressed as

$$G(s) = \begin{bmatrix} \dfrac{p_{11}}{s^2+2\zeta_1\omega_1 s+\omega_1^2} & \dfrac{p_{12}}{s^2+2\zeta_1\omega_1 s+\omega_1^2} \\ \dfrac{p_{21}}{s^2+2\zeta_2\omega_2 s+\omega_2^2} & \dfrac{p_{22}}{s^2+2\zeta_2\omega_2 s+\omega_2^2} \end{bmatrix} \tag{2}$$

for a simple 2×2 system, where the p_{ij} represent the individual elements of P.

To characterize the degree of interaction between the two subsystems represented by the transfer matrix $G(s)$, a novel coupling parameter c is defined. If the natural frequencies ω_1 and ω_2 are nearly the same, the off-diagonal elements of $G(s)$ can be represented in terms of the diagonal elements as follows:

$$p_{12} = c\alpha p_{11} \tag{3}$$

$$p_{21} = c\beta p_{22} \tag{4}$$

where α and β are scaling constants that normalize the value of c. A small value of c indicates a diagonally dominant system, whereas a larger value of c indicates significant subsystem interaction.

The stability properties of a decentralized control system coupled through the actuators can be defined in terms of the coupling parameter c. For a 2×2 system, the decentralized controller acts only on the diagonal elements of $G(s)$. $G(s)$ can be rewritten as $G_{\text{diag}}(s)(I+M(s))$, where $G_{\text{diag}}(s)$ contains only the diagonal elements of $G(s)$. The matrix $M(s)$ is called the interaction matrix, which can be represented as

$$M(s) = \begin{bmatrix} 0 & c\alpha \\ c\beta & 0 \end{bmatrix} \tag{5}$$

The stability of the coupled system can be determined by the stability of the diagonal controlled subsystems if $\det(I+M(s)) > 0$ for all s on the Nyquist contour.[3] This condition is both necessary and sufficient to ensure stability of the coupled system using diagonal controllers.

The restrictions on degree of coupling to maintain decentralized stability can be determined by evaluating $\det(I+M(s)) = 1-c^2\alpha\beta > 0$. Thus, the critical degree of coupling c^*, where the coupled system just goes unstable, is given by $c^* = \sqrt{1/\alpha\beta}$. This critical coupling value occurs when the product of the off-diagonal terms of P equals the product of the diagonal terms, that is, $p_{11}p_{22} = p_{12}p_{21}$. If the coupling exceeds this critical value, the coupled system goes unstable even though the diagonal elements of the control system are stable. For values of c greater than c^*, the open-loop plant is dominated by the off-diagonal terms. Thus, the role of the inputs can be interchanged to give a diagonally dominant system, having similar stability properties.

The stability of a centralized control scheme can be determined by inspecting the controllability matrix as the coupling parameter c changes. When critical coupling is reached ($c = c^*$) and when the natural frequencies are closely spaced ($\omega_1 \cong \omega_2$), several columns of the controllability matrix are linearly dependent, indicating that part of the system is uncontrollable. This situation means that for $c = c^*$ and $\omega_1 \cong \omega_2$, the closed-loop feedback system has one set of poles that correspond to open-loop poles that lie on the imaginary axis for near-zero damping. Thus, with any state feedback controller designed to place the poles of the coupled system, the closed-loop poles will approach the imaginary axis as c approaches c^* from either direction. Therefore, a single centralized state feedback controller cannot remain stable for both $c < c^*$ and $c > c^*$ as long as the natural frequencies are lightly damped and closely spaced.

Controller Design

A simple proportional-derivative (PD) controller is used as the decentralized control strategy. A state feedback regulator based on pole placement is used as the centralized controller. Each of these control laws can be written as

$$F(s) = -K(s)Y(s) \tag{6}$$

where $K(s)$ has terms like $K_{pi} + K_{di}s$ as each element for centralized control and as diagonal elements only for decentralized control. The closed-loop poles for the entire system, including the effect of coupling, can be determined from

$$\det[I + G(s)K(s)] = 0 \tag{7}$$

where $G(s)$ is defined in Eq. (2). The individual controller gains are determined to place these closed-loop poles at desired locations for either the diagonal subsystems with decentralized control or the entire system for centralized control. In this case, poles at $s = -17.5 \pm j30.3$ were specified, giving a well-damped response with damping ratio of 0.5 and settling time of 0.5 s.

Experimental Structure

A simple test structure has been designed and built to allow experimental verification of the stability analysis. This structure consists of a cantilever beam with disk attached to the free end (see Fig. 1a). The beam has a rectangular cross section with aspect ratio 4:1 to bring the torsional natural frequency closer to the bending natural frequencies without requiring a large disk diameter.[5] The fundamental natural frequencies in the stiffer bending direction and in torsion are each approximately 5 Hz.

Three voice-coil-type DC motors are mounted below the disk to generate control forces against a plate attached to the bottom of the disk. These linear motors generate a peak force of roughly 15 N (3.4 lbs). One of the motors is used to generate a bending force in the stiffer bending direction, and the other pair of actuators generates a twisting moment for torsion. A unique feature of the experimental setup is that the three actuators can be located anywhere along the diameter of the disk. In this way, an arbitrary degree of interaction between bending and torsion can be achieved simply by relocating the motors.

A set of three inductive-type proximity sensors are used to measure bending and torsion deflections. All of these sensors are mounted near the cantilever end of the beam. One sensor is mounted at 13.3 cm below the cantilever end against the narrow edge of the beam to measure bending deflections. A pair of sensors is mounted at 21.0 cm below the cantilever end

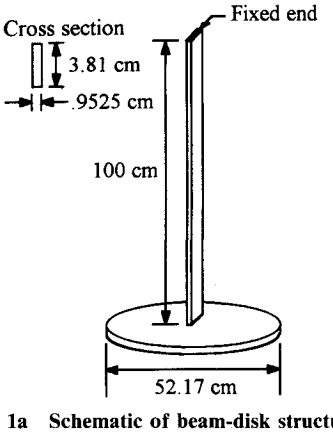

Fig. 1a Schematic of beam-disk structure.

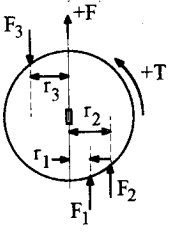

Fig. 1b Locations of actuator forces to achieve coupling.

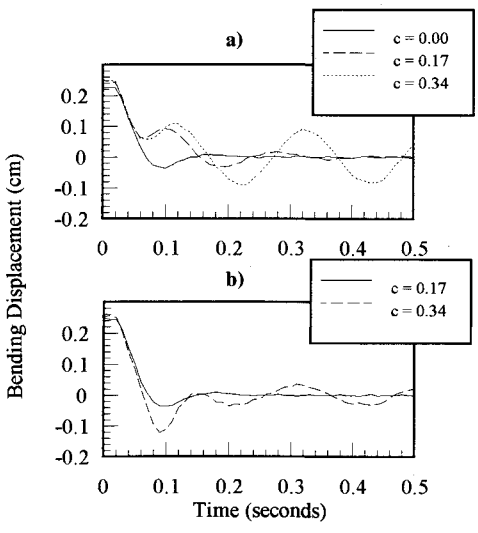

Fig. 2 Experimental responses using a) diagonal controllers and b) centralized controller.

on opposite sides of the wide edge of the beam to measure the twist angle. Using these measurements, and the deflection equations for a simple cantilever beam, the displacements at the end of the beam are determined. Velocities are calculated using finite differences.

The transfer function between bending deflection Y_b at the end of the beam and bending force F_b is given by

$$\frac{Y_b(s)}{F_b(s)} = \frac{0.0034}{s^2+0.21s+891}\left(\frac{\text{m}}{\text{N}}\right) \tag{8}$$

The transfer function between twist angle Φ at the end of the beam and twist torque T is given by

$$\frac{\Phi(s)}{T(s)} = \frac{0.47}{s^2+0.16s+987}\left(\frac{\text{rad}}{\text{Nm}}\right) \tag{9}$$

These transfer functions represent the diagonal elements of $G(s)$ in Eq. (2) and assume that a pure bending force F_b and pure twist torque T are applied. To represent coupled system behavior, off-diagonal elements are introduced into $G(s)$ by appropriately offsetting the three linear actuators so that each motor produces both a bending force and a twisting moment. The resulting configuration of forces is shown in Fig. 1b, as seen in a top view of the disk.

The total force acting in the bending direction and the total torque in torsion can be expressed in terms of the moment arms r_1, r_2, and r_3 as follows:

$$\begin{pmatrix} F_{\text{total}} \\ T_{\text{total}} \end{pmatrix} = \begin{bmatrix} 1 & \frac{1}{2}\left(\frac{1}{r_2}-\frac{1}{r_3}\right) \\ r_1 & 1 \end{bmatrix} \begin{pmatrix} F_b \\ T \end{pmatrix} \tag{10}$$

where $F_b = F_1$ and $T = r_2F_2 + r_3F_3$ represent the bending force and torque provided by the control law. Thus, the control forces (F_b and T) generate resulting actuator forces (F_{total} and T_{total}) that couple the bending and torsion subsystems, with the moment arms r_1, r_2, and r_3 completely determining the degree of coupling.

The combined transfer matrix between output displacements (Y_b and Φ) and control forces (F_b and T) can thus be represented as follows:

$$G(s) = \begin{bmatrix} \frac{Y_b(s)}{F_b(s)} & \frac{1}{2}\left(\frac{1}{r_2}-\frac{1}{r_3}\right)\left(\frac{Y_b(s)}{F_b(s)}\right) \\ r_1\frac{\Phi(s)}{T(s)} & \frac{\Phi(s)}{T(s)} \end{bmatrix} \tag{11}$$

Table 1 Actuator placement to achieve coupling

Coupling	Moment arms, m		
c	r_1	r_2	r_3
0.00	0.00	0.15	0.15
0.17	0.042	0.201	−0.15
0.34	0.085	0.023	0.050

where the diagonal transfer functions are given by Eqs. (8) and (9). The coupling parameter c can be defined in terms of the moment arms r_1, r_2, and r_3 as follows:

$$c\alpha = \frac{1}{2}\left(\frac{1}{r_2}-\frac{1}{r_3}\right) \tag{12}$$

$$c\beta = r_1 \tag{13}$$

For convenience, the scaling factors α and β have been selected so that the off-diagonal terms of $G(s)$ in Eq. (11) are equal. Also, the coupling parameter c has been normalized so that it has a value of 1 when the maximum physically achievable coupling value is reached, that is, when $r_1 = 0.25$ m, the maximum radius of the disk. Thus, $\alpha = 34.2$ (1/m) and $\beta = 0.25$ (m), resulting in a critical coupling value $c^* = 0.34$. Values for the moment arms required to generate several different coupling values on the experimental structure are given in Table 1.

Experimental Results

Experimental responses to initial conditions have been obtained for the controlled system using both decentralized and centralized controllers. A simultaneous bending deflection of 0.25 cm and a twist angle of 0.45 deg were initially provided by appropriately energizing the control actuators. The resulting initial condition responses are given in Fig. 2, showing bending deflection at the disk as deduced from proximity sensor data. (The responses in torsion have similar characteristics but are not shown for brevity.)

Experimental responses were obtained with diagonal controllers for the structure exhibiting coupling values of $c = 0$, 0.17, and 0.34 (see Fig. 2a). When no coupling is present in the system, the diagonal controllers generate responses consistent with the desired pole locations. As coupling increases, the system responses become more oscillatory until they become marginally stable at $c = 0.34$. Experimental responses using a centralized controller designed for $c = 0.17$ were also obtained for the structure exhibiting coupling values of $c = 0.17$ and 0.34 (Fig. 2b). The system responses again match the desired well-damped behavior when the actual system coupling $c = 0.17$. However, when the system coupling changes to its critical value, $c = 0.34$, the system becomes marginally stable when using the centralized controller designed for $c = 0.17$. This occurs even though the subsystem natural frequencies are not exactly equal.

Both decentralized and centralized controllers generate marginally stable responses at $c = 0.34$. Thus, the predicted critical coupling value is quite accurate, especially when considering that the experimental system includes a number of characteristics not considered in the analysis, such as higher modes, nonproportional structural damping, and nonlinearities in the mounting brackets.

Conclusions

The objective of this research is to directly investigate the role of coupling on the stability and performance of decentralized controllers. A stability analysis for systems that are coupled by the actuators has been presented. A novel coupling parameter that characterizes the degree of coupling in a 2×2 system has been introduced and defined. The representation of the degree of coupling in terms of a single parameter allows the stability and the performance robustness of both decentralized and centralized control systems to be characterized in terms of the coupling parameter for a variety of coupled sys-

tems. Higher-order systems can be analyzed in a similar manner by defining a separate coupling parameter for every pair of subsystems.

A simple test structure consisting of a cantilever beam with attached disk has been used to experimentally verify the stability analysis. This structure exhibits bending and torsion at nearly the same frequency. The force actuators can be relocated so that the degree of coupling between bending and torsion can be easily adjusted. Initial condition responses on this structure for several coupling values confirm that the performance severely degrades as the degree of coupling approaches the critical value, where the system becomes unstable for both decentralized and centralized controllers. Thus, to ensure stable control, the actuators should be located so that the coupling they induce is sufficiently different from the critical value.

Acknowledgments

The research described in this document was made possible in part by funds from an NEC Fellowship to Peter H. Meckl, provided by NEC Corporation, Tokyo, Japan. We also gratefully acknowledge Haruo Shimosaka from Meiji University, Kawasaki, Japan, for helping with the design and analysis of the test structure.

References

[1]Sandell, N. R., Jr., Varaiya, P., Athans, M., and Safonov, M. G., "Survey of Decentralized Control Methods for Large Scale Systems," *IEEE Transactions on Automatic Control,* Vol. AC-23, No. 2, 1978, pp. 108–128.

[2]Wang, S.-H., and Davison, E. J., "On the Stabilization of Decentralized Control Systems," *IEEE Transactions on Automatic Control,* Vol. AC-18, No. 5, 1973, pp. 473–478.

[3]Nwokah, O. D. I., and Perez, R. A., "On Multivariable Stability in the Gain Space," *Automatica,* Vol. 27, No. 6, 1991, pp. 975–983.

[4]Iftar, A., and Özgüner, Ü., "Local LQG/LTR Controller Design for Decentralized Systems," *IEEE Transactions on Automatic Control,* Vol. AC-32, No. 10, 1987, pp. 926–930.

[5]Horner, J. B., Meckl, P., and Shimosaka, H., "Modeling and Design of a Structure for Decentralized Active Vibration Control," *Active Noise and Vibration Control—1990,* ASME NCA-Vol. 8, ASME Winter Annual Meeting, Dallas, TX, 1990, pp. 153–159.

Design of Robust Quantitative Feedback Theory Controllers for Pitch Attitude Hold Systems

David E. Bossert*
U.S. Air Force Academy, Colorado 80840

Introduction

THE importance of robust controllers is seen by their application to situations involving plant or transfer function uncertainty. Plant uncertainty can arise from variations in plant dynamics throughout a performance range or from the inability to accurately model a complicated plant. Quantitative Feedback Theory (QFT) is one technique which has proven useful in robust control applications. QFT is a unified theory that emphasizes the use of feedback for achieving the desired system performance tolerances despite plant uncertainty and plant disturbances.[1]

Received May 18, 1992; presented as Paper 92-4409 at the AIAA Guidance, Navigation, and Control Conference, Hilton Head, SC, Aug. 10–12, 1992; revision received Oct. 25, 1992; accepted for publication March 12, 1992. This paper is declared a work of the U.S. Government and is not subject to copyright protection in the United States.

*Assistant Professor, Department of Aeronautics. Member AIAA.

QFT compares favorably to other robust techniques such as H-infinity.[2] Application to stable and unstable plants as well as linear and nonlinear plants shows the versatility of the technique.[3,4] Specific applications have ranged from flight control problems[5] to PUMA-560 robotic manipulators.[6–8] Aircraft transfer functions vary with flight conditions such as speed and altitude and provide a good challenge for robust control techniques.[9]

As case studies, a business jet and an F-4 fighter jet provide an interesting comparison for the application. The dynamics for three flight conditions cause a wide range of parameter uncertainties to arise. Additionally, inclusion of a fast and a slow actuator demonstrates the actuator's effect on the performance of the aircraft.[9] The slower actuator may represent any additional lags in the system which serve to degrade aircraft performance.

The model development section details the flight conditions used to derive the plant cases. Then, military standard MIL-F-8785B provides the guidance for the development of flight performance specifications for all categories of flight. The fourth section provides a mathematical validation of the design and the fifth section provides some insight into design tradeoffs. Finally, the last section presents the conclusion.

Model Development

Aircraft dynamics change with flight conditions, and this causes flight uncertainty throughout a typical mission. For the business jet case study, three flight conditions represent the uncertainty for a flight in this test case.[9] Flight condition 1 displays the low-speed dynamics associated with landing, while flight conditions 2 and 3 exhibit high-speed subsonic cruise dynamics. Condition 2 also shows the effect of increased moment of inertia on the aircraft dynamics. A short period approximation[9] is used for the models.

Aircraft normally incorporate actuators to make required stick forces manageable for control surface deflections, especially at high dynamic pressures.[9] However, actuators contribute lag to the aircraft system. Therefore, a designer must account for these delays. To represent additional unmodeled delays in the system, two actuators are used. One has a time constant of 0.08 s and an additional actuator is modeled with a time constant of 0.10 s.

Combining three transfer functions with two actuators yields a total of six plants. These plants represent parameter uncertainty based on speed, altitude, weight, and system lag. The maximum variation is 15.787 dB between the different plants. This case study gives a representative problem for the application of QFT.

An F-4 fighter jet provides the dynamics for the second case study. The F-4 is substantially different from a business jet, in particular because of its supersonic capabilities. Flight conditions include power approach, subsonic cruise, and supersonic cruise. The aircraft dynamics vary greatly over this range of flight conditions. Table 1 lists the plants for both the business jet and the fighter jet.

Flight Performance Specifications

The most restrictive requirements are for category A in military standard MIL-F-87875B. Choosing the most restrictive ζ and ω_n results in a range of $0.932 \text{ s} < Ts_{2\%} < 4.57$ s for the business jet and $0.735 \text{ s} < Ts_{2\%} < 4.16$ s. The maximum peak for both cases, based on $\zeta_{\min}$ is 1.309.

Quantitative Feedback Theory Design

Several sources[1,3] provide the details of the QFT design procedure. The results of this design are presented here rather than the details due to space limitations. The tracking specifications developed from MIL-F-8785B serve as the tracking bounds, and the disturbance bound is arbitrarily chosen as -20 dB at all frequencies. Figure 1 shows the nominal loop transmissions that satisfy the tracking and disturbance bounds for both the business jet and the fighter jet. This results in the